Lignin-Based Covalent Adaptable Network Resins for Digital Light Projection 3D Printing

Rebecca M. Johnson[1], Karen P. Cortés-Guzmán[1], Sachini D. Perera[1], Ankit R. Parikh[2], Vijayalakshmi Ganesh[1], Walter E. Voit[2,3], Ronald A. Smaldone[1,3]*

[1]Department of Chemistry and Biochemistry, University of Texas at Dallas, 800 West Campbell Road, Richardson, Texas, 75080, United States

[2]Department of Mechanical Engineering, University of Texas at Dallas, 800 West Campbell Road, Richardson, Texas, 75080, United States

[3]Department of Materials Science and Engineering, University of Texas at Dallas, 800 West Campbell Road, Richardson, Texas, 75080, United States

KEYWORDS: 3D printing, self-healing, transesterification, lignin, dynamic covalent chemistry, covalent adaptable networks, vanillin

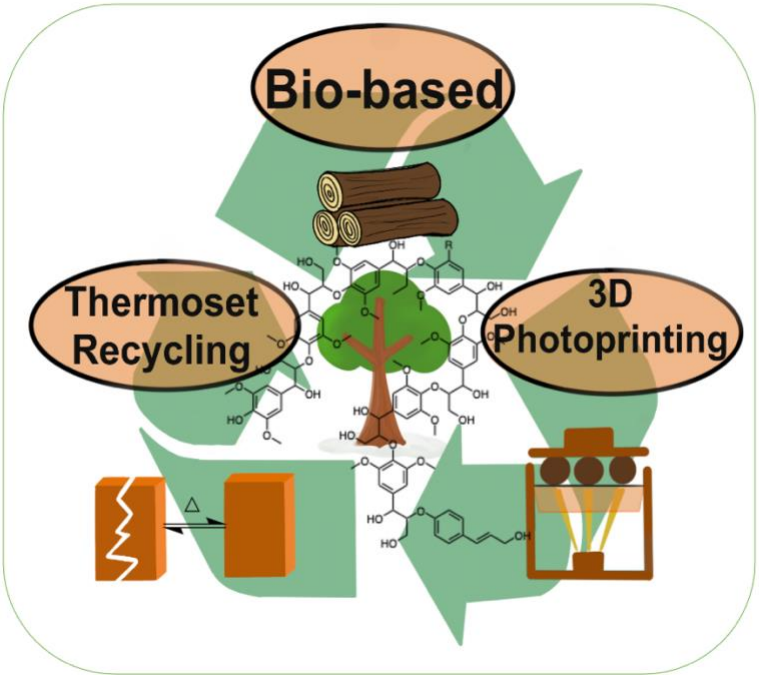

ABSTRACT: 3D printing is a low cost, customizable, and fast-growing technology with the potential to revolutionize plastic manufacturing. Vat photopolymerization 3D printing technologies stand out for their high resolution, however, the resulting printed materials are made from petroleum feedstocks and are covalently crosslinked which renders them unrecyclable. Here, resin formulations with 70 wt % bio-based content and dynamic functionality are synthesized and printed using lignin, vanillin, and soybean oil components. These printed polymers can undergo dynamic transesterification due to the methacrylated lignin (LMA) to allow for self-healing capabilities; therefore, potentially increasing the materials lifetimes

compared to traditional thermoset materials, offsetting the use of traditional petroleum-based resins, and lowering their environmental impact. The LMA also provides the thermosets with better mechanical performance and thermal stability in comparison to the controls. Additionally, compatibility with 3D printing technologies improves the competitiveness of biobased plastics with conventional materials.

1. Introduction

Plastic products are an essential part of our daily lives. While the use of plastic has given us many commodities, there are many drawbacks associated with their use. Environmental concerns from the use of petroleum, which is a non-renewable resource, have raised interest in the search for more sustainable and renewable alternatives for plastic production in recent years.[1] Another issue is that a large number of plastics that are commonly used are thermosets, which are highly crosslinked polymer networks that lack the ability to be recycled.[2] This limits their lifetime of use and creates materials that are destined to become trash in landfills.[3,4] Although thermosets cannot be recycled, they do benefit in many applications due to their low cost, strong mechanical properties, chemical and heat resistance.[5] These benefits make thermoset materials important for various applications and show no sign of diminishing use in the future.

To improve the sustainability and renewability of polymers, bio-based materials such as biomass can be utilized.[6] Biomass is defined as renewable organic material that comes from either plants or animals.[7] To use any type of biomass as an alternative to petroleum-based plastics, there are multiple aspects to consider. First, the bio-based materials must be compatible with the plastic production methods currently available, and to do so they may need to be functionalized with end groups for compatibility with polymerization techniques. Additionally, the bio-based materials must be comparable in both cost and physical properties to currently available plastics and petroleum resources to be a competitive alternative.[8,9] Two of the most abundant biopolymers are cellulose and lignin, which together are known as lignocellulosic biomass.[10,11] They can be obtained from trees and grassy plants and lignin is an abundant waste material, with over 70 million tons produced annually from the paper pulping industry.[12] Due to the abundance and ease of availability, lignocellulosic biomass is a low-cost, bio-based resource. Additionally, lignin can be valorized to give vanillin, which also can be functionalized for polymerization. Vanillin has grown to become a popular material for bio-based polymers, because of its versatility.[13,14] Soybean oil is another abundant and low-cost bio-based resource with over 50 million tons produced annually.[13,15] Acrylated epoxidized soybean oil (AESO) can be used as a UV curable coating, however it is often blended with petroleum-based monomers due to its limitations with thermal and mechanical properties and poor flowability.[13] In recent years, there have been some reports that effectively use AESO with bio-based materials such as tannic acid, vanillin, and itaconic acid.[13,15]

Lignin is an amorphous macromolecule with a rigid and highly aromatic structure mainly composed of three repeating monolignol units: sinapyl, coniferyl and p-coumaryl alcohols.[10,16] Lignin has antioxidant, UV blocking, and antimicrobial properties.[17,18] When used in polymer systems, the large aromatic monomer content of lignin can provide mechanical strength and thermal stability.[12] Lignin is separated from cellulose through several different methods, of which all give variability in structure, and the amount of hydroxyl functionality on the molecule.[19] Due to the complexity, variability and often poor solubility, lignin is mainly used as a filler or modified for compatibility in polymer systems.[10,12,17,20–23]

Additive manufacturing, or 3D printing, is a method that creates materials in a layer-by-layer manner to create a three-dimensional object.[24] 3D printing is an extremely customizable method that creates less waste compared to traditional plastic production methods.[25] Vat photopolymerization is a 3D printing technique that uses a UV or LED light source, such as a projector in digital light projection (DLP), to

polymerize liquid resin monomers in this method.[26] Most commonly the monomers will polymerize through a radical polymerization reaction, using monomers such as acrylates, methacrylates and thiol-ene click reactions.[3,27] There are multiple aspects to consider for the resin formulation design to allow for printer compatibility. The formulation should include a photoinitiator to start the radical polymerization and monomer functionality that will polymerize fast enough through a radical reaction.[25] The resin must also have a certain viscosity (typically <50 cP) to allow for the print plate to recoat in between each layer. There have been several examples of the use of lignin without modification as a filler for composites in both extrusion and photo 3D printing.[11,28–30] The work by Sutton *et al*., has incorporated up to 15 wt % methacrylated lignin into the polymeric network, utilizing commercially available resins and photoprinted the resin formulations.[28] To further improve the sustainability of lignin containing polymers, chemical designs that allow for recyclability of thermosets are desirable.

Dynamic covalent chemistry (DCC) has been used in many thermoset polymers to create materials that can recover from damage by reconfiguring covalent bonds across cracks or scratches.[25] Covalent adaptable networks (CANs) are crosslinked thermoset polymer networks that use DCC to undergo bond exchange initiated by an external stimulus, such as light, heat, or changes in pH.[31] This reversible network rearrangement allows for a macroscopic flow that can promote self-healing, reprocessing, shape memory, degradability, and stress relaxation.[2,4] Dynamic transesterification is the rearrangement of ester bonds and free hydroxyls in a polymeric network.[32] This exchange is triggered using heat and a catalyst, such as a Lewis acid.[33] With CANs, thermoset materials can be made recyclable, thereby avoiding immediate disposal in landfills. The dynamic linkages are used in conjunction with permanent crosslinks to create materials that retain their shape while self-healing.[14,34,35] The use of DCC in thermosets helps retain the mechanical properties of the networks while gaining the reprocessable properties of a thermoplastic polymer.[14,36]

Here we report a series of bio-based and 3D printable CANs that can undergo dynamic transesterification. The resins consist of bio-based lignin, vanillin, and soybean oil monomers, and are cured through a thiol-acrylate radical polymerization which is compatible with the 3D printer light source. These resins have a total of 70% by weight biobased content, which displaces a significant amount of petroleum sourced feedstocks. These materials are renewable, sustainable, thermally stable and could have extended lifetimes in comparison to traditional 3D photoprinting resins. The LMA plays a crucial role in the resins for several reasons, including improving the thermal stability, mechanical properties, and the self-healing ability. This improved thermal stability allows for more effective self-healing and recyclability in LMA containing polymers as observed through the ability to heal both scratches and complete cuts.

2. Experimental Section

2.1. Materials

All chemicals are used as received unless otherwise noted. Lignin (dealkaline), 3-mercaptopropionic acid, and phenylbis(2,4,6- trimethylbenzoyl)phosphine oxide (BAPO >96%) were purchased from TCI. Soybean oil, epoxidized acrylate (AESO) and zinc acetylacetonate hydrate was purchased from Sigma-Aldrich. 4-dimethylaminopyridine (99%, DMAP), and *p*-toluenesulfonic acid (99%) were purchased from Acros Organics. Vanillin (99%), polyethylene glycol 400, and methacrylic anhydride (94% stabilized with *ca* 0.2% 2,4-dimethyl-6-tertbutylphenol) were purchased from Alfa Aesar. Dichloromethane (DCM), sodium chloride (NaCl), sodium bicarbonate ($NaHCO_3$), sodium hydroxide (NaOH), magnesium sulfate

anhydrous ($MgSO_4$), toluene, isopropanol and chloroform were purchased from Fisher Scientific. Polyethylene glycol 600 (PEG-OH 600) was obtained from Mallinckrodt.

2.2. Characterization

Nuclear magnetic resonance (NMR) spectroscopy was performed using a Bruker 600 MHz AVANCE spectrometer for ^1H spectra at 25°C in $CDCl_3$ or DMSO-d_6.

Fourier transform infrared spectroscopy (FTIR) was performed on a Cary 600 series using an attenuated total reflection (ATR) apparatus at 25°C with a resolution of 2 cm^{-1} and was recorded in the 4000-400 cm^{-1} range with 32 scans per sample.

2.3. Resin Formulations

The composition of all resin formulations is shown in Table 1. All components were mixed (except for the photoinitiator) and then were probe sonicated for varying time periods. T2 75 soft resin was probe sonicated for 30 s at 30W and T3 50, T3 75 and T2 75 hard resins were probe sonicated for 60 s at 60W. After probe sonication, the photoinitiator (2 wt % of BAPO) was added and the resin was ultrasonicated until the photoinitiator dissolved, typically around 30 min.

2.4. 3D Printing

All samples were printed using a Photon Zero digital light projection (DLP) 3D Printer at 405 nm. The printed specimens for tensile testing were ASTM D638 standard specimen type V. Compression discs were printed with a diameter of 10mm. Once printed, unreacted excess resin was washed off using isopropanol and then they were post-cured under a 405 nm lamp for 24 h.

2.5. Thermal Characterization

Thermogravimetric analysis (TGA) was performed on a Mettler Toledo SDT using 5-10 mg samples loaded in an alumina crucible and was conducted with a heating rate of 10°C/min, from 25°C to 700°C under N_2 atmosphere with a flow rate of 100 mL/min.

Differential scanning calorimetry (DSC) was performed using a Mettler Toledo DSC using 5-10 mg samples loaded into alumina crucibles. The heating and cooling rate was 10°C/ min from -40°C to 200°C with N_2 as the cell purge gas.

2.6. Mechanical Testing

Tensile and compression testing was performed using an Instron 5848 Micro Tester and Instron 6800. The load cells were either 50 N or 500 N. The test specimens were ASTM D638 standard type V, and a 10mm/min extension rate was applied for all tests until failure.

For compression testing of the printed and reprocessed discs, 10mm cylindrical discs were used (10mm diameter and height). The samples were tested using an Instron 6800 universal testing machine with a 50 kN load cell.

2.7. Gel Content and Swelling Tests

Square samples were cut from 3D printed parts that were printed and post cured as previously described. The initial weight of the samples was recorded, and they were placed in either toluene or methanol for 24h. The samples were dried and weighed to determine the percent swelling. The samples were then dried in a vacuum oven at 80°C for 24h and the final weight was recorded to determine gel content.

2.8. Annealing, Self-Healing and Reprocessing

Annealing was performed by exposing the printed samples to thermal treatment at 80°C for 24h in an oven. Healing experiments were performed on both the as printed and annealed samples. Self-healing was tested by both scratch and break tests. The samples were either gently scratched on the surface or cut in half at a 45° angle using a razor blade. Then, they were put under slight pressure by placing them between glass slides and held together with binder clips. For scratch tests, they were placed in the oven at 140°C, for 12h, and then 160°C overnight, for 12h if healing did not occur at 140°C. For the healing of cuts, samples were placed in the oven at 140°C, for 24h. Optical microscopy was used to obtain both the before and after images of the healing experiments.

The samples were reprocessed using a Carver hydraulic hot press. The specimens were mechanically ground and pressed at 2,000 psi (2 metric tons) at 140°C for a period of 4h in a circular metal mold to create discs which were then used for compression testing.

3. Results and Discussion

3.1. Synthesis of Monomers and Resins

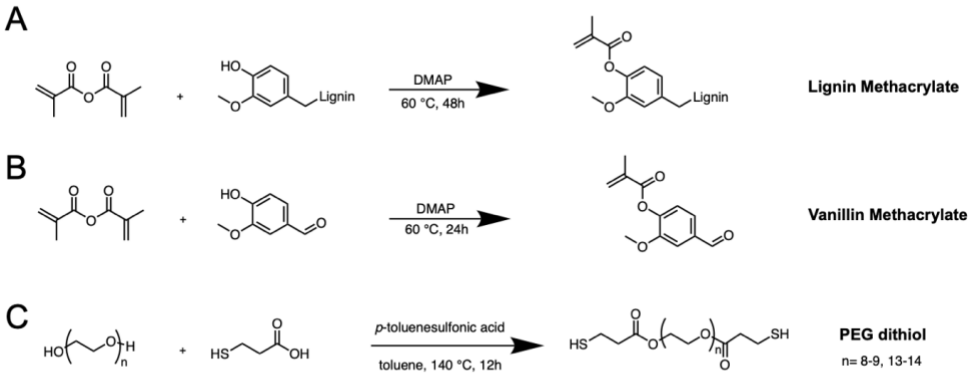

Scheme 1. Synthetic procedures for (A) lignin methacrylate (B) vanillin methacrylate and (C) PEG-dithiol reactions using both PEG-400 and PEG-600.

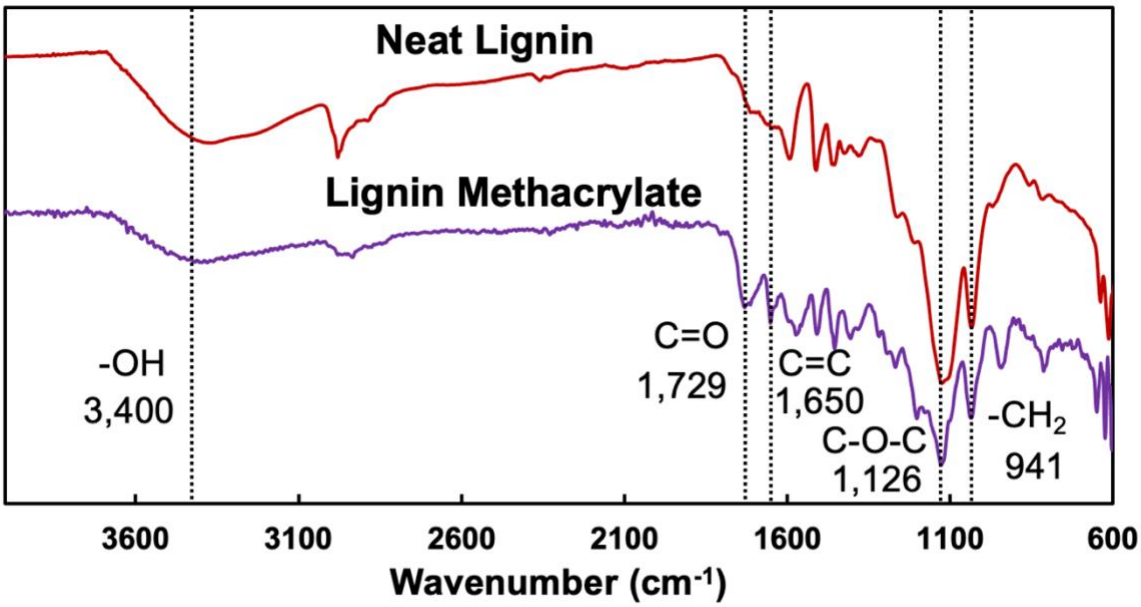

Figure 1. FTIR spectra of unfunctionalized lignin (top) and methacrylated lignin (bottom), showing successful functionalization of lignin with methacrylate groups.

The synthesis of each resin component is shown in **Scheme 1**. Lignin and vanillin were functionalized with photoreactive methacrylate groups through a method as previously reported.[28,34] Lignin was reacted with methacrylic anhydride, and the product was characterized by FTIR, as shown in **Figure 1**. The reaction progress can be monitored by the decrease of hydroxyl groups and the appearance of methacrylate functional groups. The -OH stretching peak at 3,400 cm^{-1} decreases, but does not completely disappear, which is important as there is a retention of free hydroxyls in the polymer network that can undergo transesterification. The peaks for the C=O stretches can be seen at 1,729 cm^{-1}, the C-O-C stretches at 1,126 cm^{-1} and the $-CH_2$ bending at 941 cm^{-1}. Both PEG-600 and PEG-400 were reacted with 3-mercaptoproionic acid to give thiol functional groups on both ends of the PEG chains by using a previously reported procedure.[11]

Table 1. Printed resin formulations with varying ratios of biobased monomers. T2 formulations contain PEG-400 dithiol and T3 formulations PEG-600 dithiol.

Formulation	AESO (mol %)	PEG dithiol (mol %)	VMA (mol %)	LMA (wt %)	BAPO (wt %)	Zn Catalyst (wt %)
T2 75 soft	4.60	20.30 PEG-600	75.11	2.5	2	2
T2 75 hard	4.60	20.30 PEG-600	75.11	2.5	2	2
T3 50	12.01	22.55 PEG-400	65.44	2.5	2	2
T3 75	4.73	17.8 PEG-400	77.47	2.5	2	2

The formulations were made using different chain lengths of PEG dithiol crosslinkers and by altering the ratio of the bio-based monomers. The resin ratios can be seen in **Table 1**. The T2 formulations use PEG-600 dithiol and T3 formulations use PEG-400 dithiol. The molar ratio of thiol to acrylate/methacrylate functional groups was kept constant, while changing the ratio of VMA to AESO between formulations. At room temperature, VMA is a crystalline solid, which is gently heated to give a liquid for complete incorporation into the resin. A high ratio of VMA to AESO was used to give improved stiffness and tensile strength to the resins, while providing sufficient flowability to enable compatibility with the 3D printer. All formulations include 2 wt % of BAPO as the photoinitiator and 2 wt % of the $Zn(acac)_2$ as the transesterification catalyst. No UV photoblockers were needed in the formulations, as lignin has UV-blocking properties of its own.[18] LMA is a solid light brown powder and has poor solubility in the resin systems. Due to the poor solubility, the lignin was incorporated at 2.5 wt % into the resin blends. Larger amounts became difficult to dissolve and incorporate into the resin. To improve this, the resins were probe sonicated to help dissolve the LMA.

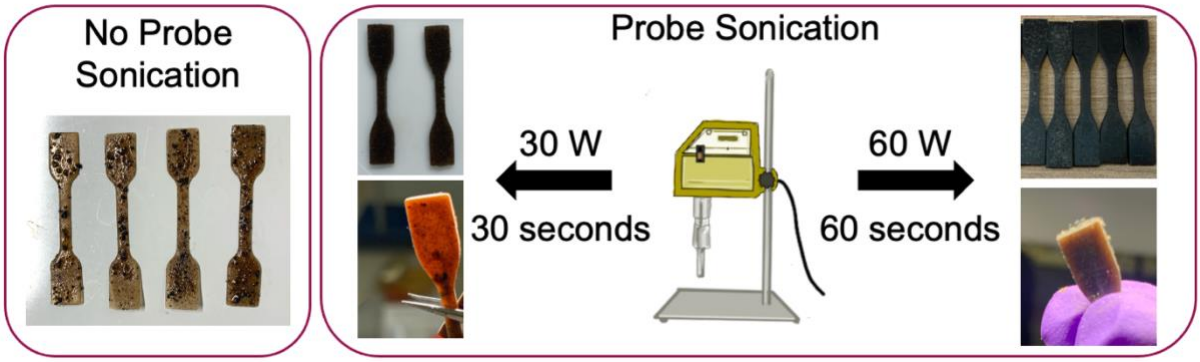

Figure 2. Comparisons of printed T2 75 samples without probe sonication (left), T2 75 soft probe sonicated at 30 W for 30 s (middle) and T2 75 hard probe sonicated at 60 W for 60 s. Probe sonication of the resins before printing improves the dispersion of LMA. Higher amounts of time and power provided improved incorporation of methacrylated lignin into the resin, where T2 75 soft is improved compared to the non-probe sonicated resin but still has large, visible particles when compared to T2 75 hard.

The formulations were mixed using a probe sonicator at either 30 W for 30 s or 60 W for 60 s. By increasing both probe sonication times and power intensities, there was an improvement in the dispersion of the lignin within the resins as seen in **Figure 2**. The probe sonication decreased the size of the lignin particles resulting in better homogeneity and improved crosslinking between the resin and the LMA. In the formulations with the shorter time and power of probe sonication, the lignin was still not fully incorporated. As a result, only one of the formulations at 30 W probe sonication was tested as a comparison to the resins probe sonicated at higher power and longer time periods. T2 75 probe sonicated at 60 W for 60 s is denoted as T2 75 hard and T2 75 probe sonicated at 30 W at 30 s is denoted as T2 75 soft. We hypothesize that the formulations with less sonication allowed for the LMA to crosslink only somewhat with the monomers, and that the uncrosslinked LMA acts primarily as a plasticizer in the network. In the formulations with higher time periods and power of probe sonication, the LMA incorporated almost completely and created a nearly homogeneous resin with little to no visible particles.

All formulations saw complete incorporation of the zinc catalyst with probe sonication except for T3 50. Very little of the catalyst dissolved in this formulation, leaving a solid clump behind that was removed from the formulation before 3D printing. Overall, T3 50 had poor incorporation of both LMA and catalyst into the resin. With this formulation, there is a lower amount of VMA compared to the other formulations, which seems to play an important role in solubilizing the LMA. VMA is similar in structure and is derived from lignin, so it helps to improve overall incorporation of LMA into the resin. Additionally, control formulations were created, consisting of either 2.5 wt % of unmodified lignin, or no lignin following the ratios shown in Table 1. The resins with the unmodified lignin had very poor solubility with the particles of lignin being distributed inconsistently throughout.

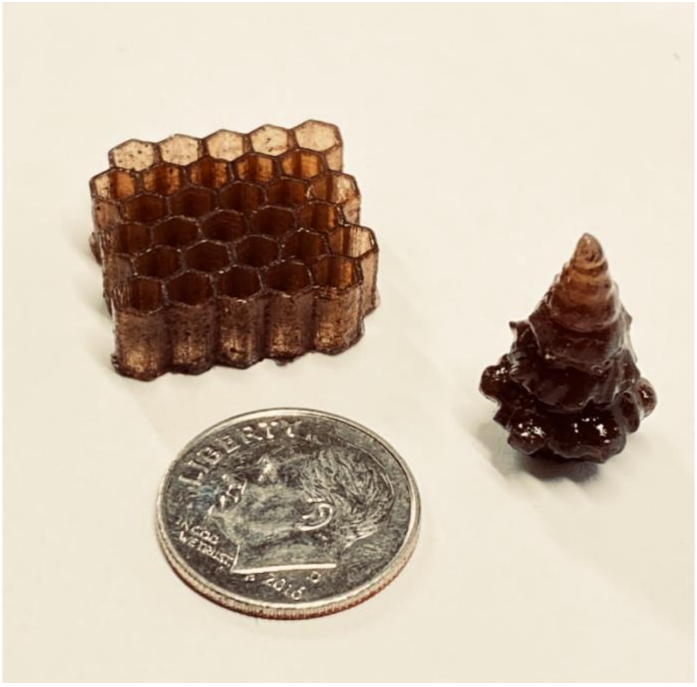

Figure 3. Examples of objects 3D printed using T2 75 H resin to demonstrate the print resolution and even dispersion of the LMA. A honeycomb and a tree are shown with a U.S. dime included as a reference.

For the printing of the formulations, dog bone specimens, compression discs, and complex structures such as a honeycomb, and tree were printed to show that the formulations provide very good printing accuracy (**Figure 3)**.

3.2. Thermal Properties

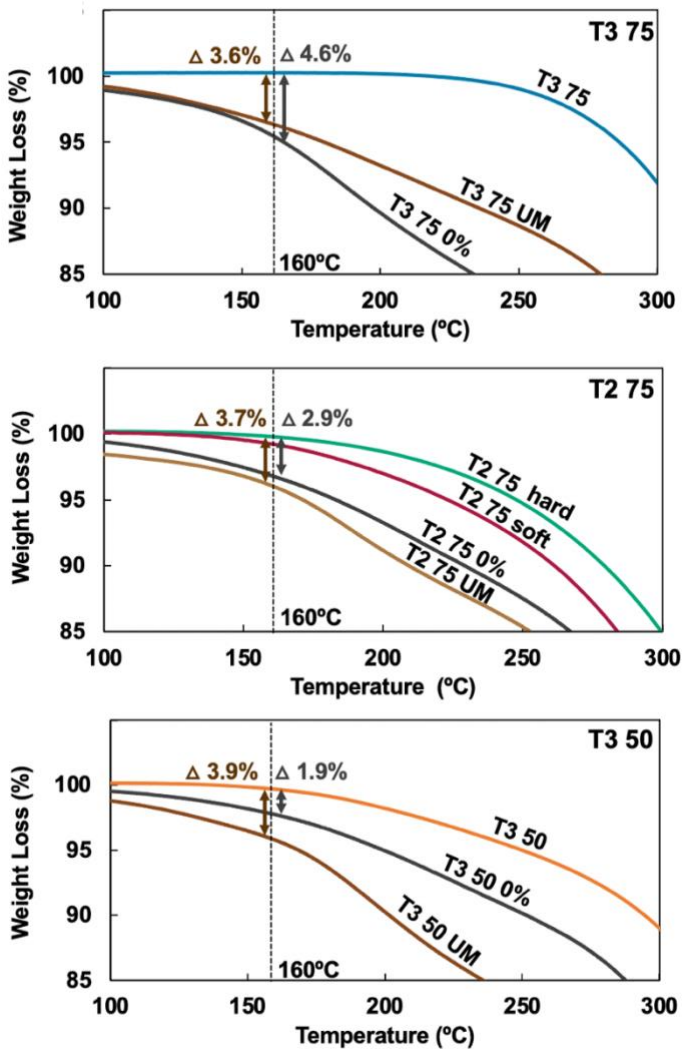

Figure 4. Thermogravimetric analysis of the three formulations showing the percent of mass lost at 160°C, with T3 75 (top), T2 75 (middle) and T3 50 (bottom) all showing increased thermal stability with LMA included as an additive. Thermal stability at this temperature is important because it is in the range of where transesterification can occur, and the materials must be stable with minimal degradation for effective self-healing to occur.

Thermogravimetric analysis (TGA) was performed to determine the thermal stability of the polymer systems. It has been previously reported that functionalized lignin can increase the thermal stability of polymers.[35–37] The formulations with LMA showed the highest thermal stability, with a 5% weight loss temperature significantly above the temperature range for transesterification. **Figure 4** shows the expanded curves of the formulations, with each plot comparing the formulations with LMA to those with unmodified lignin (UM) and the controls with no lignin (0%). The onset of degradation, 5% weight loss, is used to determine the stable temperature range for evaluating the self-healing and reprocessing behavior. The formulations with LMA showed the highest thermal stability, with a 5% weight loss temperature significantly above the temperature range for transesterification. For T2 75 soft the 5% weight loss

temperature is 243 ºC, for T2 75 hard 228 ºC, for T3 50 243 ºC and for T3 75 283 ºC. These materials are stable in the range of 140°C-160 °C, which is where the materials can self-heal. The control formulations with UM lignin and without lignin however, started to show degradation in the range of 150-190 °C (Figure 4). This lower onset of weight loss compromises the stability of the control formulations at the temperatures required for transesterification reactions to occur. LMA provides an increased thermal stability to the materials, which allows for self-healing with minimal degradation. The glass transition temperatures (T_g) were determined using differential scanning calorimetry (DSC). The glass transition temperatures for the formulations with no lignin and unmodified lignin were similar, however the formulations with LMA were all higher than their respective controls (Figure S6, S7 and S8). This is a good indication of increased crosslinking within the polymer network and suggests incorporation of LMA into the resin backbone. Additionally, T3 50 and T2 75 hard formulations show two less well-defined transitions for the T_gs, which is a sign of a copolymer system. This is indicative of parts of the LMA being polymerized into the network and parts of it remaining uncrosslinked, resulting in two phases within the network.

3.3. Self-healing Studies

To evaluate the dynamic functionality of the resins, all formulations were tested with both scratch and break tests. Scratch tests show the ability to heal small cuts while full breaks can show larger scale healing and evaluate the healing through the recovery of mechanical properties. The rate of the network exchange is influenced by the catalyst type and concentration, backbone stiffness of the polymer, and the crosslinking density.[30,31] Incorporating DCC can extend the lifetime of the material and lessen the detrimental environmental effects through improved reprocessability. Multiple materials have incorporated lignin into CANs, focusing often on reactions such as Diels-Alder and transesterification.[4,32,38–42] The use of lignin in a 3D photoprintable resin with dynamic functionality is yet to be explored.

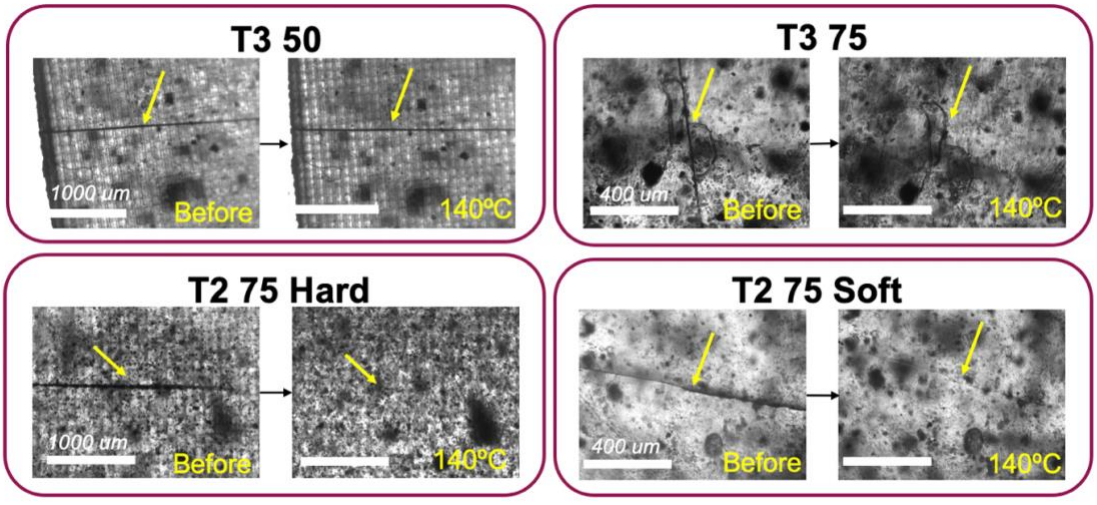

Figure 5. Optical microscope images of scratch tests of the four formulations showing before and after heating at 140 °C for 24 h to evaluate self-healing. All formulations except for T3 50 can completely heal a scratch on the surface of the material. The T3 50 likely lacks this ability due to poor incorporation of LMA and catalyst into the precursor resin.

The formulations with LMA have many esters and free hydroxyls from lignin's structure that can participate in transesterification reactions. The dynamic nature of transesterification, catalyzed by $Zn(acac)_2$, should allow for the closure of cracks and damage in the polymeric network. With this in mind, self-healing of complete cuts and scratches should be possible for the dynamic resins. The scratches were healed for 24 h at 140 °C. However, for the scratch tests all formulations except T3 50 could heal the cracks. The complete disappearance of the cracks in T3 75, T2 75 hard and T2 75 soft can be seen in **Figure 5**. The T3 50 had poor incorporation of the catalyst after probe sonication, which shows the importance of the catalyst solubility for these formulations for transesterification to be successful. The poor incorporation plays a role on the self-healing and emphasizes the importance of choice in monomers to help improve incorporation of both LMA and the zinc catalyst.

For the self-healing of the controls, only 140 °C was used due to the early onset of degradation of the materials determined by TGA. Both the unmodified lignin and without lignin controls were discolored and severely cracked after heat treatment. They also showed no healing of the cracks at 140 °C (Figure S9). The images of the samples with unmodified lignin are difficult to view due to the large amount of unincorporated lignin particles in the polymer. While the control with UM lignin has free hydroxyls and ester functionality, it appears to not be enough dynamic functionality to allow for healing to occur. The stability of the materials is important for extended use, and the LMA is responsible for the increased stability required for self-healing of the materials.

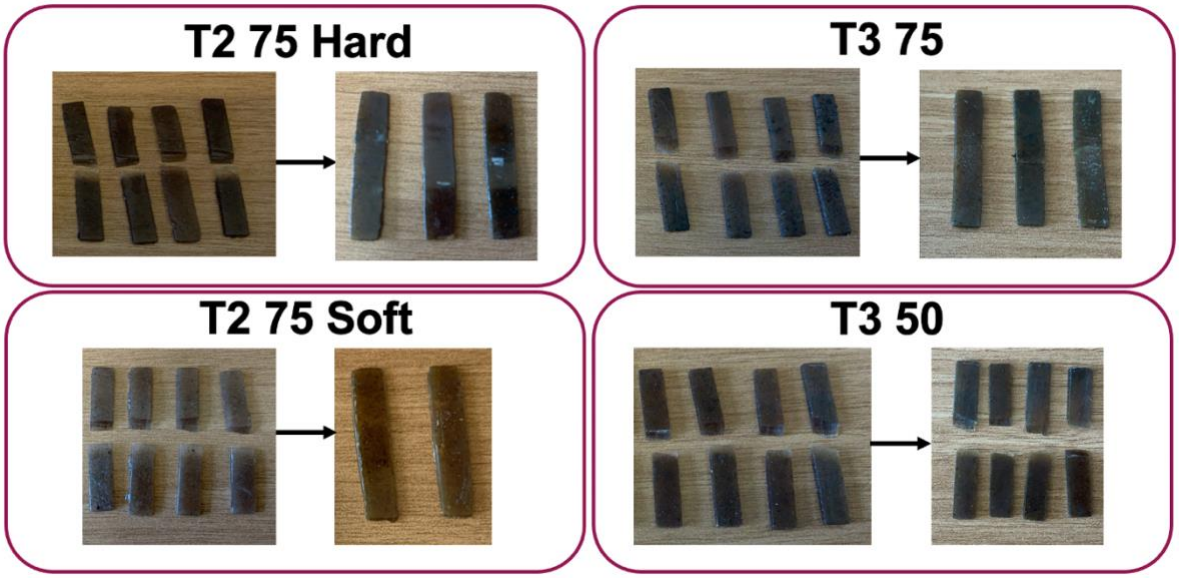

Figure 6. Images of cut samples before and after being healed for all formulations. The self-healing tests were carried out at 140 °C for 24 h. All formulations can heal complete cuts, except for T3 50 which mirrors its inability to heal surface scratches.

The formulations were also tested for their ability to fully self-heal a complete cut. As printed strips were cut at an angle to create a higher amount of touching surface area for self-healing. The cut and healed strips can be seen in **Figure 6**. The strips were able to heal in a trend that mirrors the self-healing of the scratches. The T3 50 formulation was completely unable to heal any cuts, while T2 75 soft, T2 75 hard and T3 75 healed well. For T2 75 soft, the scars from the cut are almost impossible to discern with the visible eye.

3.4. Mechanical Properties

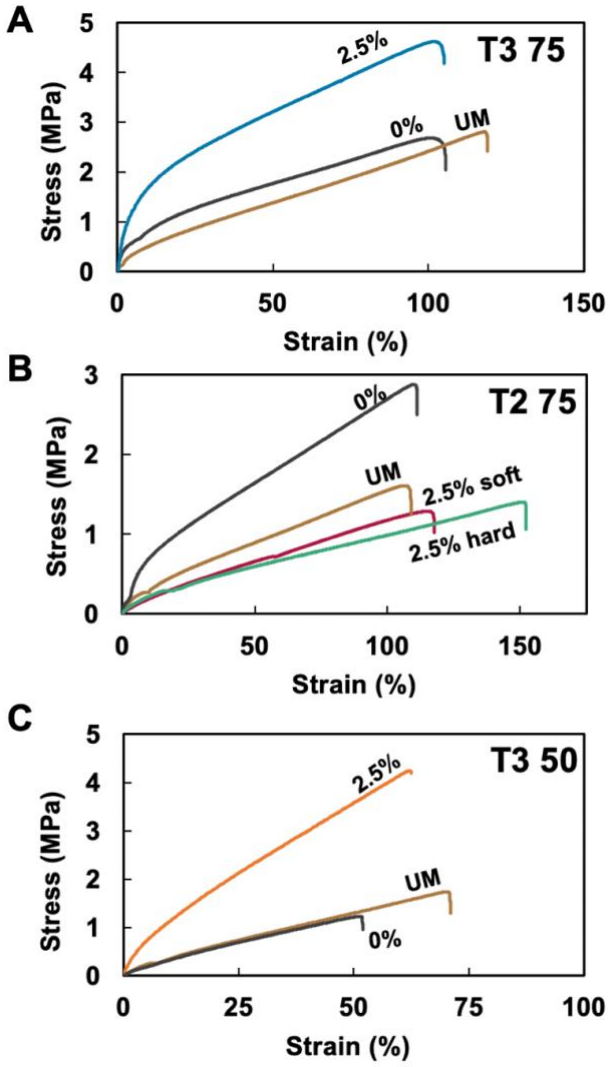

Figure 7. Representative stress-strain curves for each formulation and their controls with unmodified lignin (brown) and no lignin (grey) with T3 75 after 60 W at 60 s (A), both T2 75 hard and soft, under both sets of probe sonication conditions (B), and T3 50 after 60 W at 60 s (C). The mechanical data of the 30 W 30 s formulations of T3 50 and T3 75 are included in the supporting information in comparison to their respective 60 W 60 s probe sonicated formulations (Figures S10 and Figure S11).

The mechanical properties of the 3D printed formulations and their annealed and healed samples were all evaluated through tensile testing. The samples were all annealed to allow for the network to relax any stresses within the polymer chains and to help reduce the number of unreacted polymerizable groups. At least six samples for each formulation were tested to evaluate Young's modulus, ultimate tensile strength and strain at break. Mechanical properties were obtained for as printed samples, annealed samples and samples that were first annealed and then allowed to self-heal for comparisons. The changes in mechanical properties for the differing time and power intensities of probe sonication were also evaluated, as well as

the control samples that do not contain lignin and those with unmodified lignin. Representative curves of the stress-strain data are shown in **Figure 7** comparing the formulations to their controls with UM lignin and without lignin. For the controls, we hypothesize that the unmodified lignin acts as a plasticizer; additionally, the printed materials have inconsistent properties likely due to poor dispersion of the UM lignin in the resin (Figure 7).

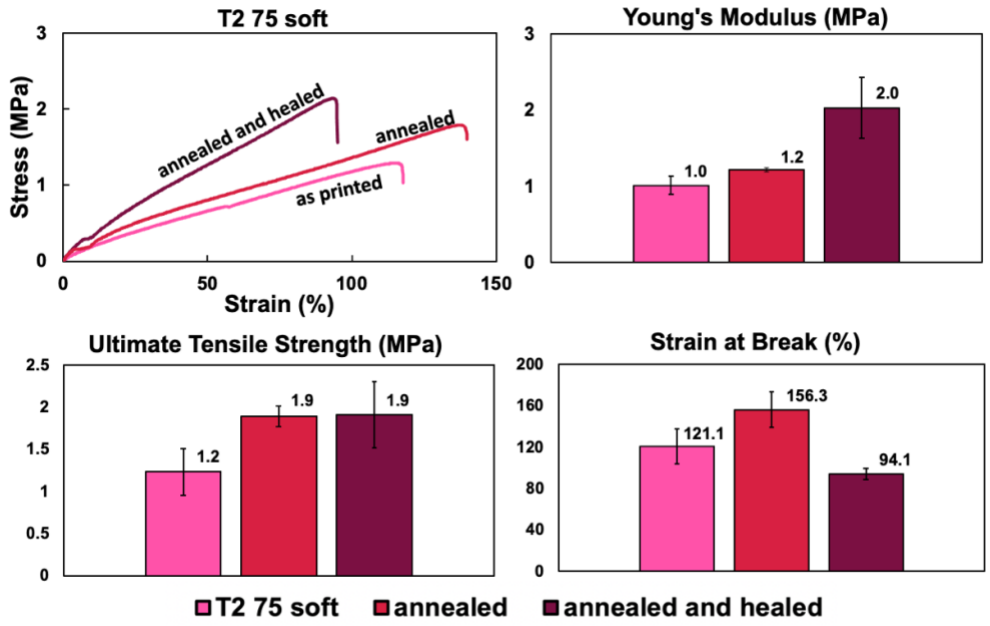

Figure 8. Comparison of mechanical properties of as printed, annealed, and annealed then healed samples of T2 75 soft

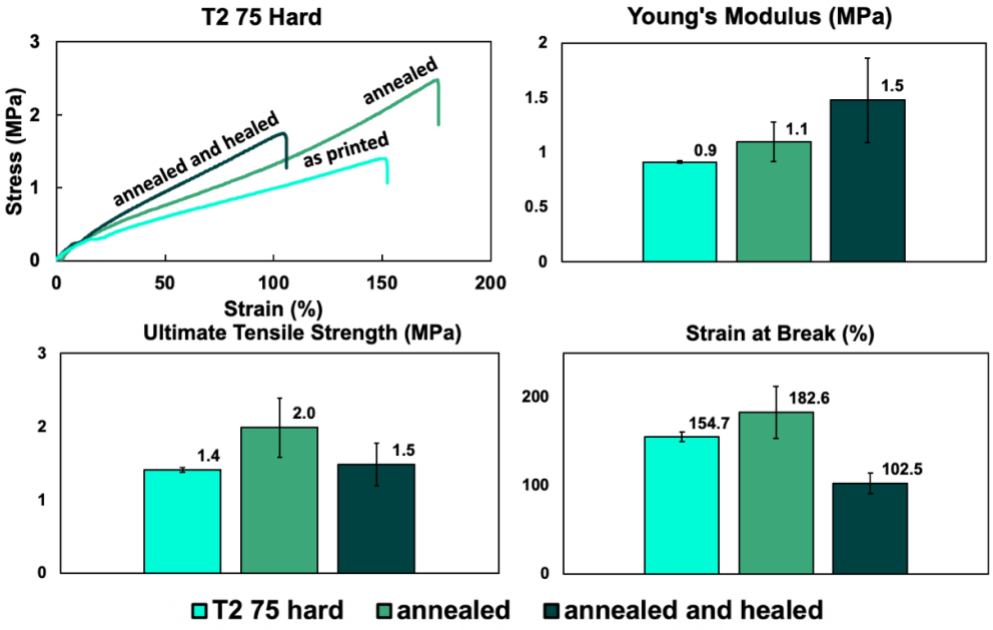

Figure 9. Comparison of mechanical properties of as printed, annealed, and annealed then healed samples of T2 75 hard

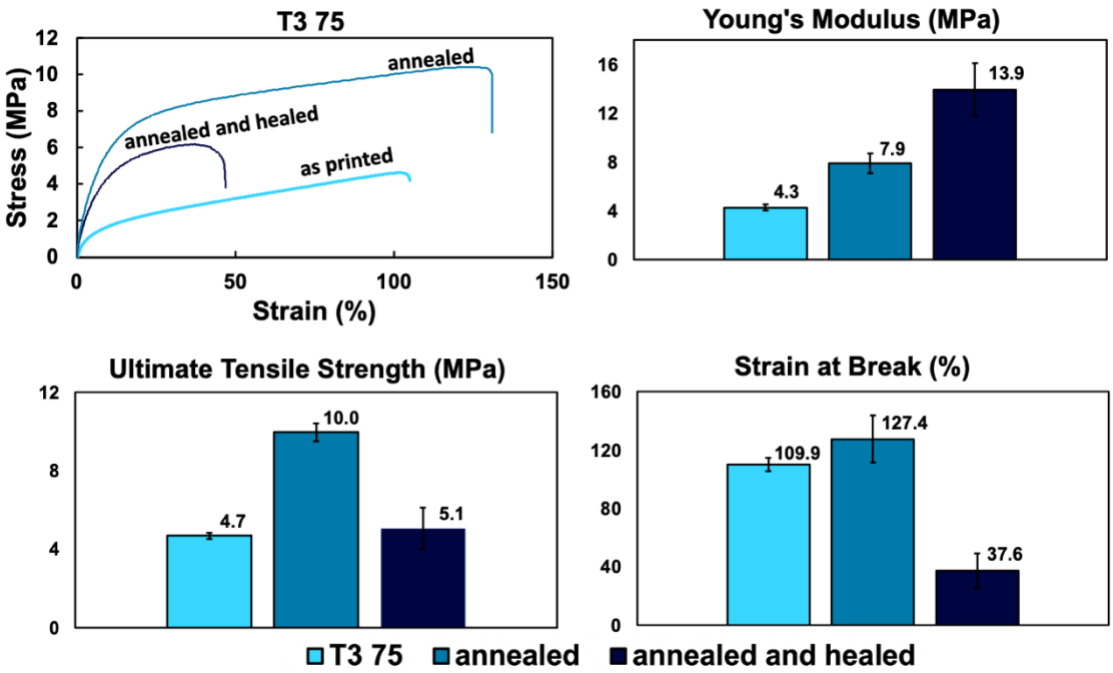

Figure 10. Comparison of mechanical properties for the as printed, annealed, and annealed then healed samples of T3 75

Annealed samples were thermally treated at 80 °C for 24 h. To quantify the extent of polymerization of annealed formulation samples, gel content was determined by swelling in methanol and toluene (Figure S16 and S17). All formulations with LMA have nearly 90% or higher gel content, showing high conversion from monomers to the polymer network. The comparison of as printed samples to annealed samples along with the annealed then healed samples can be seen in **Figure 8** for T2 75 soft, **Figure 9** for T2 75 hard and **Figure 10** for T3 75. However, T3 50 did not show as much improvement after annealing compared to the other formulations (Figure S15). We hypothesize that due to poor incorporation of LMA, the formulation could not fully polymerize with unreacted methacrylate groups within the poorly dispersed LMA particles. Both **Table 2** and **Table S1** show the change in mechanical properties after annealing.

Table 2. Mechanical property values and healing efficiencies of the annealed and healed samples. NO: healing not observed.

Annealed Formulations	UTS (MPa)	UTS after healing (MPa)	UTS recovery (%)	Strain at break (%)	Strain at break after healing (%)	Strain at break recovery (%)	Young's Modulus (MPa)	Young's Modulus after healing (MPa)	Young's Modulus recovery (%)
T2 75 Soft	1.89 (±0.1)	1.91 (±0.4)	101%	156.29 (±18.1)	94.11 (±5.1)	60%	1.22 (±0.1)	2.03 (±0.4)	166%
T2 75 Hard	1.99 (±0.4)	1.49 (±0.3)	75%	182.58 (±29.3)	102.48 (±11.8)	56%	1.09 (±0.2)	1.48 (±0.4)	136%
T3 75	9.96 (±0.45)	5.06 (±1.06)	51%	127.39 (±16.02)	37.59 (±11.76)	30%	7.89 (±0.82)	13.93 (±2.16)	177%
T3 50	2.5	NO	NO	73.4	NO	NO	3.5	NO	NO

The mechanical properties of the annealed samples were also compared to the mechanical properties of the annealed samples after they had undergone self-healing. After healing, all samples except for T3 50 had fully mended their cuts. Scars were not observed on T2 75 formulations, while they could still be seen on T3 75. Controls were not tested for complete cuts, as they could not heal scratches and are not thermally stable at self-healing temperatures. When testing the mechanical properties, the samples did not break on the original cut location. The healed formulations were able to recover their mechanical properties in comparison to the annealed values. The recovery can be seen in **Table 2.** T3 50 was unable to heal at all, so it could not recover any of the mechanical properties to be evaluated. Between the T2 75 formulations, T2 75 soft healed better as it recovered more of its strain at break and ultimate tensile strength. T3 75 did not heal as well as the T2 75 samples and this is likely due to the network being stiffer and resulting in less mobility of the chains to allow for complete healing through transesterification.

To give insight on the lifetime of the dynamic resins, the formulations were all reprocessed into new parts to show recyclability. The resins were mechanically ground and formed with a hydraulic press (Figure S16). All formulations could form new discs, except T3 50, which again is most likely due to the poor solubility of the zinc catalyst. To show overall longevity of the resin, T2 75 hard was reprocessed multiple times and the mechanical properties of each cycle was evaluated (Figure S15 and Figure S17). The first cycle of grinding and reprocessing saw poor incorporation, but the next three cycles showed full incorporation of the mechanically ground pieces. An initial drop of mechanical properties is seen after the first cycle of reprocessing; however, the successive cycles retain their compressive modulus. This retention of mechanical properties after multiple cycles of reprocessing is likely due to the LMA providing thermal stability to the formulation.

4. Conclusion

Several CAN resin formulations were synthesized with bio-based materials such as lignin, vanillin, and soybean oil. The resins were compatible with DLP photoprinting and could be used to create complex printed parts. These formulations incorporated up to 70% by weight bio-based content to displace the use of petroleum-based resins and included dynamic covalent bonds that could undergo transesterification. The transesterification was able to occur with the use of methacrylated lignin, which provided an abundant number of free hydroxyls and ester functionality into the polymeric network. By incorporating LMA with the use of probe sonication and annealing the samples, several properties of the resins were significantly improved compared to controls that do not contain LMA, such as mechanical properties and thermal stability, and thus allowing for the materials to self-heal effectively. The enhanced thermal stability from the LMA allows for self-healing and improved recyclability of the materials compared to traditional thermosets with reduced degradation after being subjected to temperatures for transesterification to occur. Additionally, the formulations with the LMA were able to be self-healed and recycled effectively through scratch tests, full break tests and hot press reprocessing. The control formulations showed no self-healing, reinforcing the importance of the LMA in the formulations. These materials have high bio-based content, are thermally stable and exhibit self-healing behaviors that could potentially increase their lifetimes in comparison to non-self-healable 3D photoprinting resins.

Acknowledgements

K.C.G. acknowledges the Consejo Nacional de Ciencia y Tecnología (CONACYT, Mexican Council of Science and Technology) for doctoral fellowship. We also acknowledge the Advanced Polymer Research Lab (APRL) at UT Dallas for access to facilities for the thermal characterization of polymers. UT Dallas. A.K.P. acknowledges scientific and internship support from the U.S. Food and Drug Administration. R.A.S. acknowledges support from UT Dallas, and the Army Research Laboratory (W911SR-22-C-0048).

Email: Ronald.smaldone@utdallas.edu

References

(1) Moreno, A.; Sipponen, M. H. *Mater. Horiz.* **2020**, *7*, 2237–2257.

(2) Zhang, S.; Liu, T.; Hao, C.; Wang, L.; Han, J.; Liu, H.; Zhang, J. *Green Chem.* **2018**, *20*, 2995–3000.

(3) Durand-Silva, A.; Smaldone, R. A. *ACS Cent. Sci.* **2020**, *6*, 836–838.

(4) Sheppard, D. T.; Jin, K.; Hamachi, L. S.; Dean, W.; Fortman, D. J.; Fortman, D. J.; Ellison, C. J.; Dichtel, W. R. *ACS Cent. Sci.* **2020**, *6*, 921–927.

(5) Chen, J.; Liu, H.; Zhang, W.; Lv, L.; Liu, Z. *J Appl Polym Sci* **2020**, *137*, 1–11.

(6) Thakur, V. K.; Thakur, M. K.; Raghavan, P.; Kessler, M. R. *ACS Sustain. Chem. Eng.* **2014**, *2*, 1072–1092.

(7) Birch, K.; Tyfield, D. *Sci. Technol. Hum. Values.* **2013**, *38*, 299–327.

(8) Sternberg, J.; Sequerth, O.; Pilla, S. *Prog. Polym. Sci*. **2021**.

(9) Bass, G. F.; Epps, T. H. *Polym. Chem.* **2021.** 4130–4158.

(10) Jawerth, M.; Johansson, M.; Lundmark, S.; Gioia, C.; Lawoko, M. *ACS Sustain. Chem. Eng.* **2017**, *5*, 10918–10925.

(11) Liu, H.; Mulderrig, L.; Hallinan, D.; Chung, H. *Macromol. Rapid Commun.* **2021**, *42*.

(12) Ebers, L. S.; Arya, A.; Bowland, C. C.; Glasser, W. G.; Chmely, S. C.; Naskar, A. K.; Laborie, M. P. *Biopolymers*. 2021, 1–12.

(13) Chen, J.; Liu, H.; Zhang, W.; Lv, L.; Liu, Z. *J. Appl. Polym. Sci.* **2020**, *137*.

(14) Cortés-Guzmán, K. P.; Parikh, A. R.; Sparacin, M. L.; Remy, A. K.; Adegoke, L.; Chitrakar, C.; Ecker, M.; Voit, W. E.; Smaldone, R. A. *ACS Sustain. Chem. Eng.* **2022**, *10*, 13091–13099.

(15) Dai, J.; Liu, X.; Ma, S.; Wang, J.; Shen, X.; You, S.; Zhu, J. *Prog. Org. Coat.* **2016**, *97*, 210–215.

(16) Adler, E. *Wood Sci. Technol.* **1976**.

(17) Hajirahimkhan, S.; Xu, C. C.; Ragogna, P. J. *ACS Sustain. Chem. Eng.* **2018**, *6* (11), 14685–14694.

(18) Sugiarto, S.; Leow, Y.; Tan, C. L.; Wang, G.; Kai, D. *Bioact. Mater.* **2022,** 71–94.

(19) Glasser, W. G. *Front. Chem.* **2019.**

(20) Liu, H.; Chung, H. *ACS Sustain. Chem. Eng.* **2017**, *5*, 9160–9168.

(21) Kun, D.; Pukánszky, B. *Eur. Polym. J.* **2017,** 618–641.

(22) Gkartzou, E.; Koumoulos, E. P.; Charitidis, C. A. *Manuf. Rev.* **2017**, *4*.

(23) Zhang, S.; Liu, T.; Hao, C.; Wang, L.; Han, J.; Liu, H.; Zhang, J. *Green Chem.* **2018**, *20*, 2995–3000.

(24) Quan, H.; Zhang, T.; Xu, H.; Luo, S.; Nie, J.; Zhu, X. *Bioact. Mater.* **2020**, 110–115.

(25) Durand-Silva, A.; Cortés-Guzmán, K. P.; Johnson, R. M.; Perera, S. D.; Diwakara, S. D.; Smaldone, R. A. *ACS Macro Lett.* **2021**, *10*, 486–491.

(26) Prabhakar, M. M.; Saravanan, A. K.; Lenin, A. H.; Leno, I. J.; Mayandi, K.; Ramalingam, P. S. *Mater. Today: Proc,* **2020**, *45*, 6108–6114.

(27) Konuray, O.; Fernández-Francos, X.; Ramis, X.; Serra, À. *Polymers*, **2018**.

(28) Sutton, J. T.; Rajan, K.; Harper, D. P.; Chmely, S. C. *ACS Appl. Mater. Interfaces* **2018**, *10*, 36456–36463.

(29) Nguyen, N. A.; Barnes, S. H.; Bowland, C. C.; Meek, K. M.; Littrell, K. C.; Keum, J. K.; Naskar, A. K. *Sci. Adv.* **2018**, *4*, 1–15.

(30) Nguyen, N. A.; Bowland, C. C.; Naskar, A. K. *Data Br.* **2018**, *19*, 936–950.

(31) Kloxin, C. J.; Bowman, C. N. *Chem. Soc. Rev.* **2013**, *42*, 7161–7173.

(32) Hao, C.; Liu, T.; Zhang, S.; Brown, L.; Li, R.; Xin, J.; Zhong, T.; Jiang, L.; Zhang, J. *Chem. Sus. Chem.* **2019**, *12*, 1049–1058.

(33) Krishnakumar, B.; Sanka, R. V. S. P.; Binder, W. H.; Parthasarthy, V.; Rana, S.; Karak, N. *Chem. Eng. J.* **2020**.

(34) Durand-Silva, A.; Cortés-Guzmán, K. P.; Johnson, R. M.; Perera, S. D.; Diwakara, S. D.; Smaldone, R. A. *ACS Macro Lett.* **2021**, *10*, 486–491.

(35) Durand-Silva, A.; Perera, S. D.; Remy, A. K.; Peng, H.-C.; Hargrove, J. A.; Ferneyhough, Z. D.; Lopez Landaverde, P. M.; Stelling, A. L.; Smaldone, R. A. *ACS Appl. Polym. Mater.* **2022**.

(36) Davidson, J. R.; Appuhamillage, G. A.; Thompson, C. M.; Voit, W.; Smaldone, R. A. *ACS Appl. Mater. Interfaces* **2016**, *8*, 16961–16966.

(37) Zhang, C.; Yan, M.; Cochran, E. W.; Kessler, M. R. *Mater. Today Commun.* **2015**, *5*, 18–22.

(38) Ye, D.; Li, S.; Lu, X.; Zhang, X.; Rojas, O. J. *ACS Sustain. Chem. Eng.* **2016**, *4*, 5248–5257.

(39) Cui, C.; Sadeghifar, H.; Sen, S.; Argyropoulos, D. S. *Lignin Polymers: Part 2*; 2013; Vol. 8.

(40) Hu, X. Q.; Ye, D. Z.; Tang, J. B.; Zhang, L. J.; Zhang, X. *RSC Adv.* **2016**, *6*, 13797–13802.

(41) Buono, P.; Duval, A.; Averous, L.; Habibi, Y. *Polymer (Guildf)* **2017**, *133*, 78–88.

(42) Gao, S.; Cheng, Z.; Zhou, X.; Liu, Y.; Wang, J.; Wang, C.; Chu, F.; Xu, F.; Zhang, D. *Chem. Eng. J.* **2020**, *394*.

(43) Liu, W.; Fang, C.; Wang, S.; Huang, J.; Qiu, X. *Macromolecules* **2019**, *52*, 6474–6484.

(44) Zhang, S.; Liu, T.; Hao, C.; Wang, L.; Han, J.; Liu, H.; Zhang, J. *Green Chem.* **2018**, *20*, 2995–3000.

(45) Liu, W.; Fang, C.; Wang, S.; Huang, J.; Qiu, X. *Macromolecules* **2019**, *52*, 6474–6484.

Supplementary Information

Lignin-Based Covalent Adaptable Network Resins for Digital Light Projection 3D Printing

*Rebecca M. Johnson[1], Karen P. Cortés-Guzmán[1], Sachini D. Perera[1], Ankit R. Parikh[2], Vijayalakshmi Ganesh[1], Walter E. Voit[2,3], Ronald A. Smaldone[1,3]**

[1]Department of Chemistry and Biochemistry, University of Texas at Dallas, 800 West Campbell Road, Richardson, Texas, 75080, United States

[2]Department of Mechanical Engineering, University of Texas at Dallas, 800 West Campbell Road, Richardson, Texas, 75080, United States

[3]Department of Materials Science and Engineering, University of Texas at Dallas, 800 West Campbell Road, Richardson, Texas, 75080, United States

*Correspondence Address
Professor Ronald A. Smaldone
Department of Chemistry and Biochemistry
The University of Texas at Dallas
800 W. Campbell Road
Richardson, Texas 75080
Phone: (+1)-972-883-6342
email: ronald.smaldone@utdallas.edu

Table of Contents

1. ^{1}H NMR spectra of synthesized compounds.....S1-2

S1. ^{1}H NMR LMA and Lignin

S2. ^{1}H NMR AESO

2. FTIR spectra of monomers, resins, and cured polymer formulations.....S3

3. TGA Curves for all formulations…….....S4

4. First derivative plots of TGA curves ….....S5

5. DSC curves for all formulations…….....S5-8

S6. T2 75 DSC

S7. T3 75 DSC

S8. T3 50 DSC

6. Optical microscopy of controls and UM samples for self-healing…….....S9

7. Mechanical properties for probe sonication…….....S10-11

S10. T3 50 formulation with and without probe sonication

S11. T3 75 formulation with and without probe sonication

8. Table of properties before and after annealing for controls……..…TS1

9. Mechanical properties both before and after annealing for T3 50 …….....S12

10. Swelling and gel content tests….....S13-14

S13. Swelling and gel content in toluene

S14. Swelling and gel content in methanol

9. Reprocessing mechanical data for T2 75 Hard….....S15

9. Mechanically ground and reprocessed samples….....S16

10. Images of reprocessed samples for T2 75 Hard….....S17

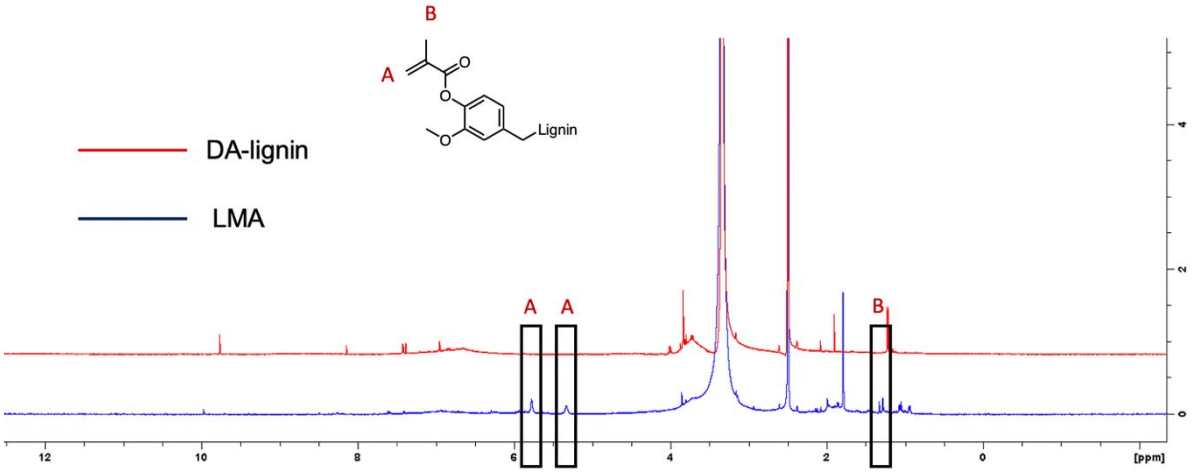

Figure S1. Dealkaline lignin and LMA ^{1}H-NMR showing functionalization with methacrylate functional groups

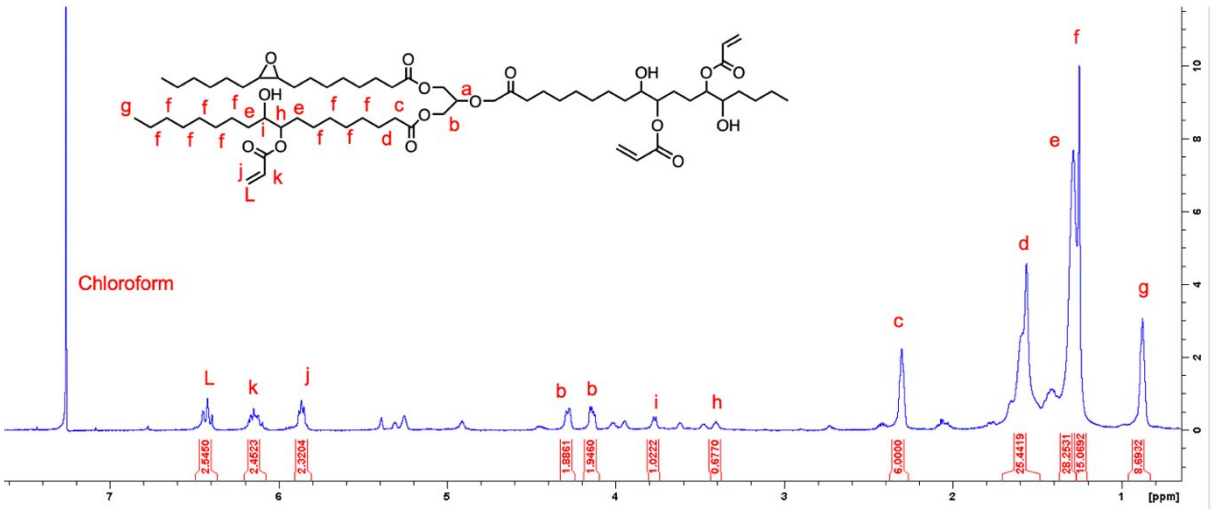

Figure S2. ^{1}H NMR of acrylated epoxidized soybean oil in $CDCl_3$

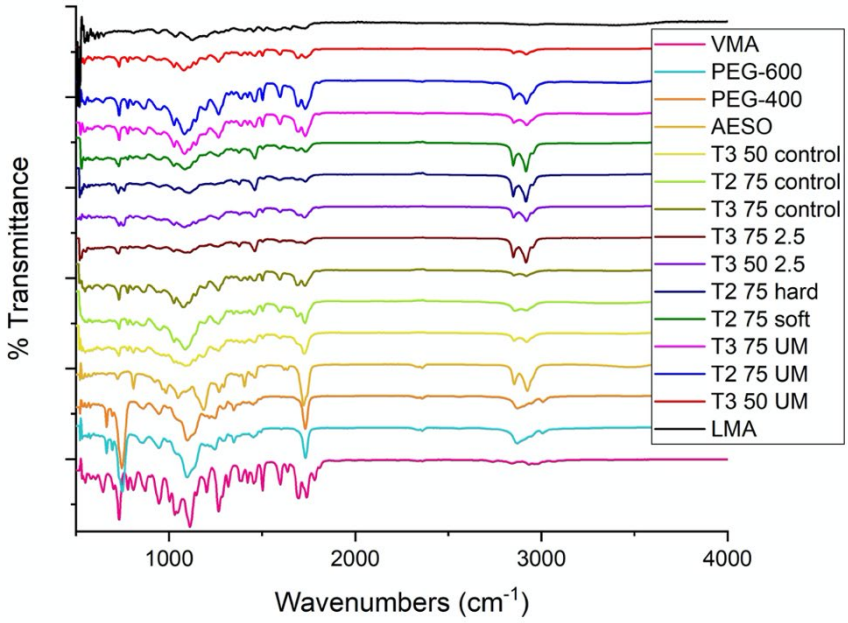

Figure S3. Overlay of the FTIR spectra for the cured resins and individual resin components.

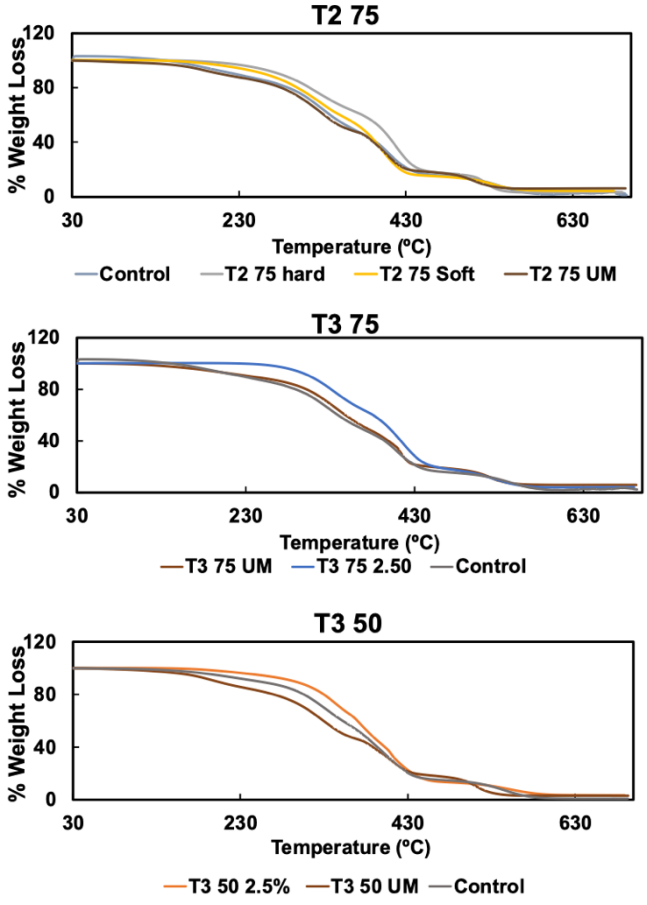

Figure S4. TGA curves of the T2 75 formulations (top), T3 75 formulations (middle), and T3 50 formulations (bottom). All curves show that the addition of LMA to the polymer formulation gives higher thermal stability compared to controls that do not have LMA.

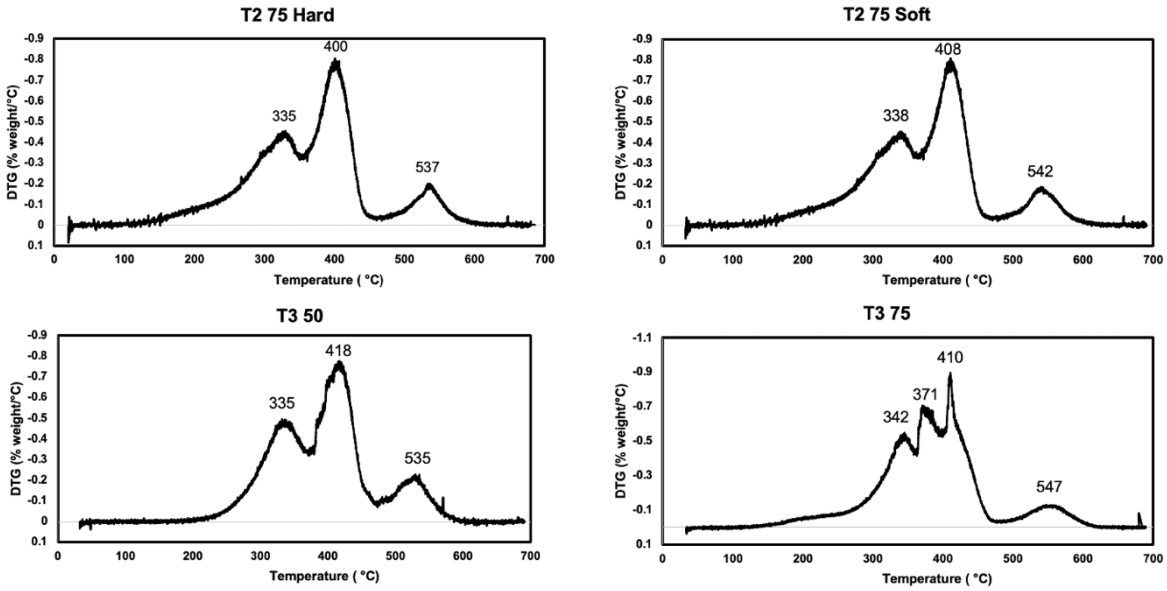

Figure S5. First derivative curves of the TGA plots for the 2.5 wt % of LMA formulations

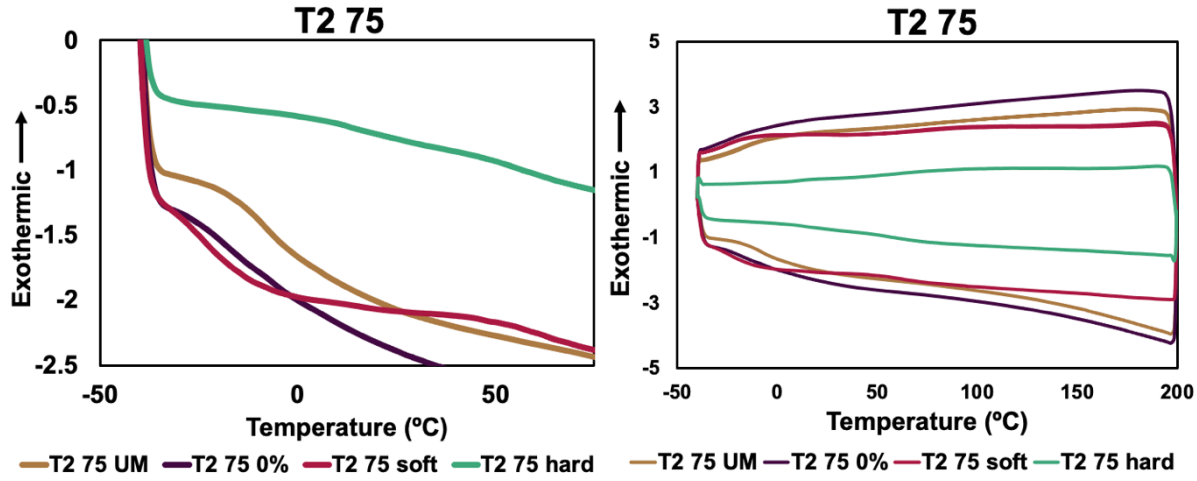

Figure S6. Expanded and full DSC for T2 75

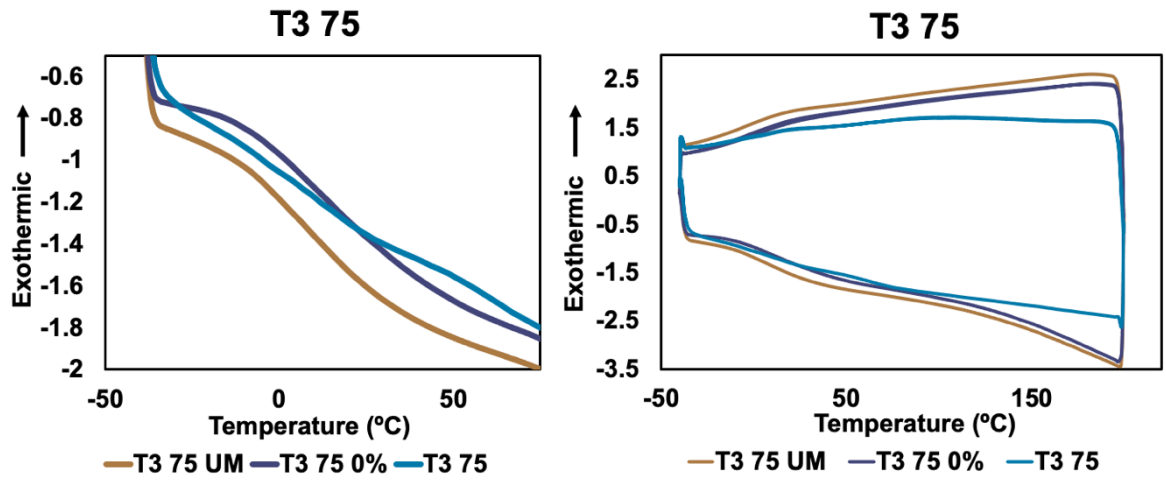

Figure S7. Expanded and full DSC for T3 75

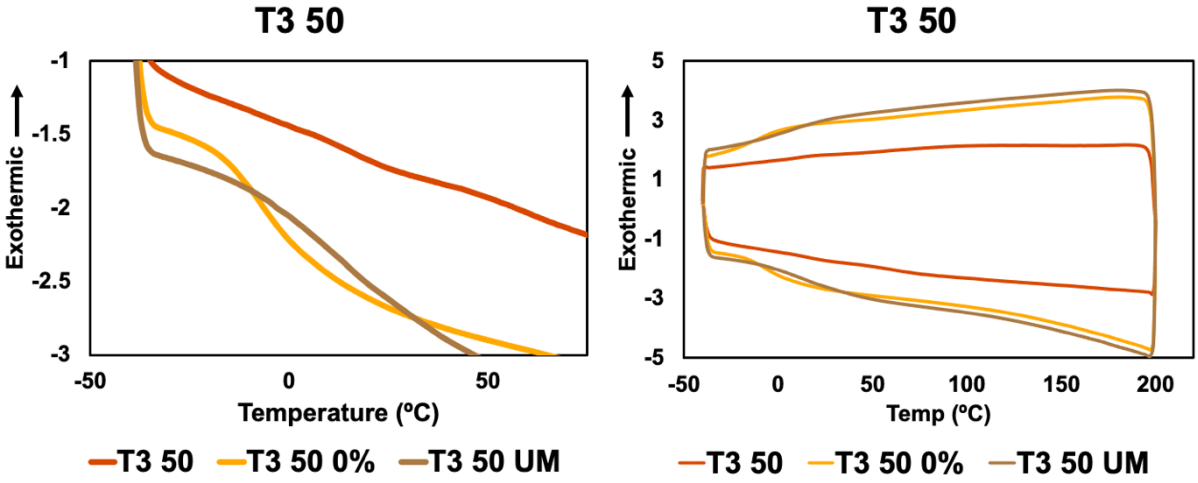

Figure S8. Expanded and full DSC for T3 50

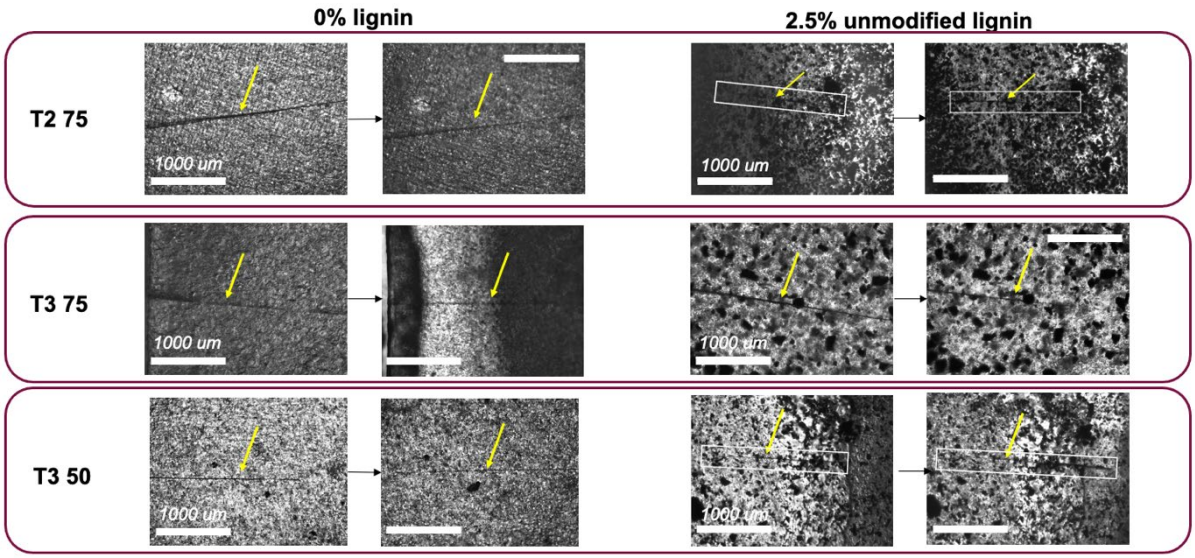

Figure S9. Optical microscope images of UM and 0% lignin controls, showing before healing and after heat treatment at 140°C for 12h.

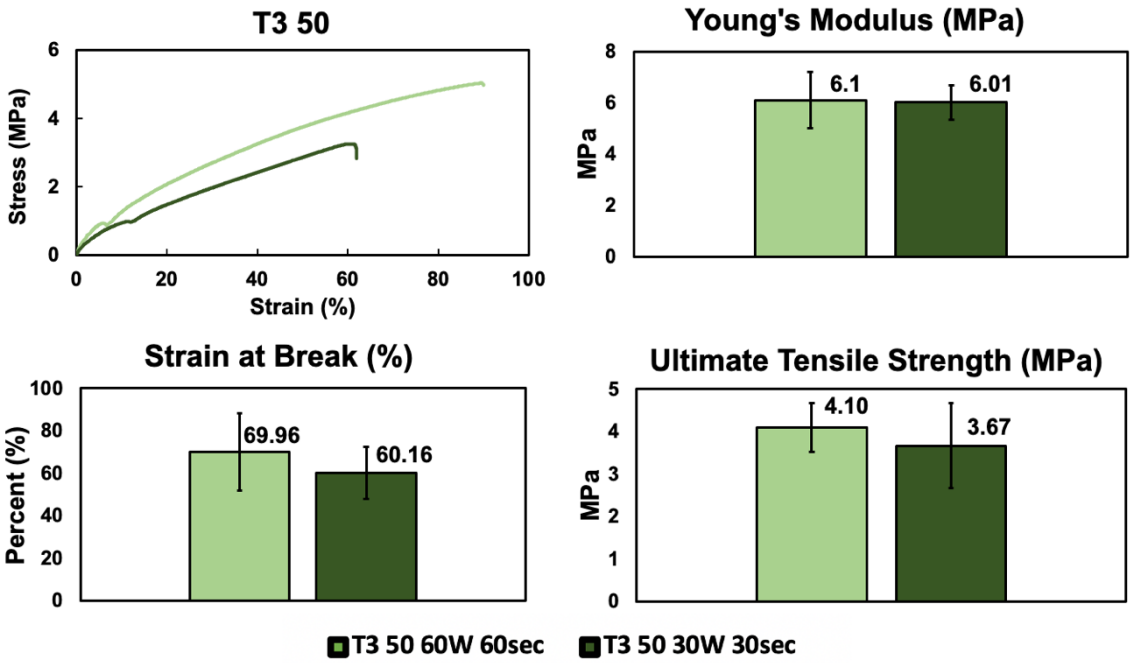

Figure S10. Representative stress-strain curves of the T3 50 formulations (A) at varying probe sonication powers and times and plots of the (B) Young's modulus, (C) strain at break, and (D) ultimate tensile strength.

Table S1. Mechanical property values for the as printed and annealed control samples.

Formulation	UTS (MPa)	UTS after annealing (MPa)	Strain at break (%)	Strain at break after annealing (%)	Young's Modulus (MPa)	Young's Modulus after annealing (MPa)
T2 75 0%	2.9 (±0.4)	1.6 (±0.2)	101.7 (±21.3)	157.9 (±12.1)	2.9 (±0.5)	1.0 (±0.1)
T2 75 UM	2.2 (±0.7)	1.5 (±0.2)	109.1 (±22.2)	164.3 (± 15.8)	2.0 (±0.5)	0.9 (±0.1)
T3 75 0%	3.0 (±0.7)	1.9 (±0.5)	96.8 (±17.0)	77.8 (±16.9)	3.2 (±0.7)	2.4 (±0.2)
T3 75 UM	3.8 (±0.7)	4.9 (±0.6)	65.4 (±13.8)	118.6 (± 20.6)	5.8 (±0.5)	4.3 (±1.2)
T3 50 0%	1.2 (±0.3)	4.3 (±0.6)	44.0 (±9.9)	167.4 (±42.8)	2.8 (±0.5)	2.4 (±0.4)
T3 50 UM	1.6 (±0.3)	2.1 (±0.2)	70.3 (±15.3)	95.3 (±6.9)	2.3 (±0.4)	2.2 (±0.3)

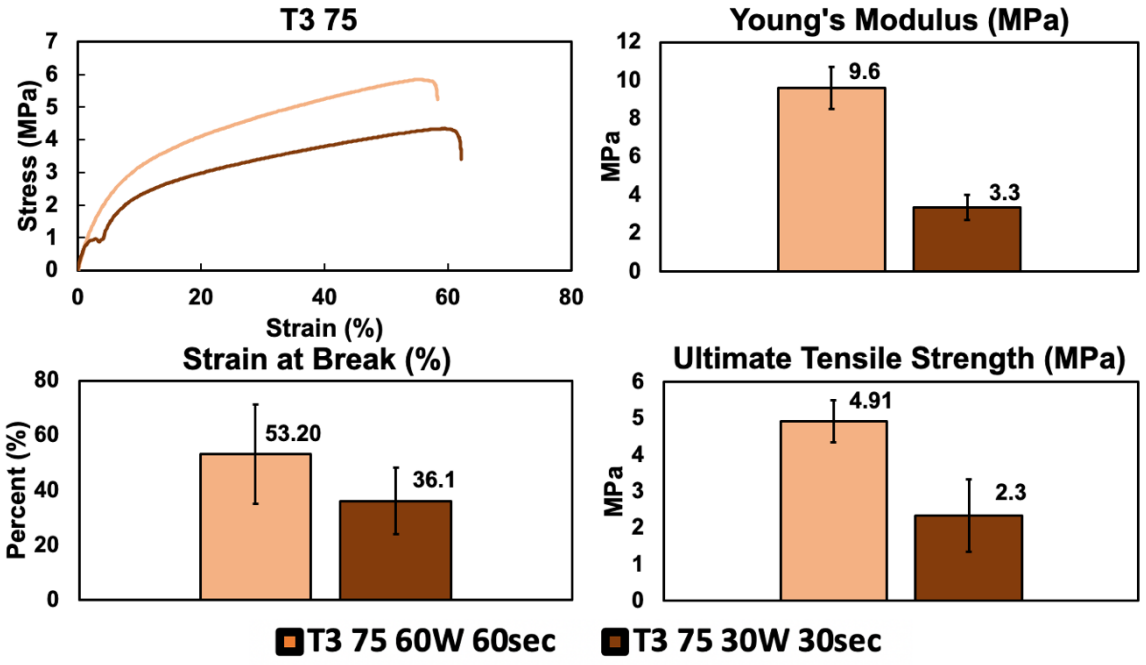

Figure S11. Representative stress-strain curves of T3 75 formulations (A) of varying probe sonication and (B) Young's modulus (C) Strain at break and (D) ultimate tensile strength

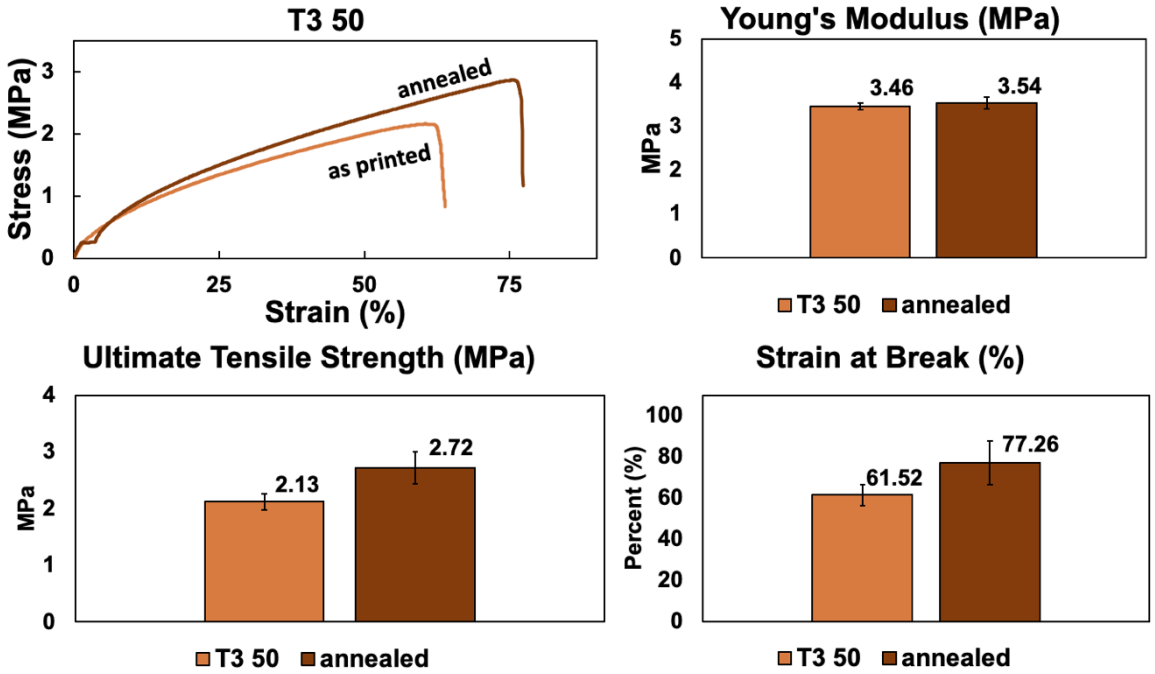

Figure S12. Mechanical properties of T3 50 for both as printed and annealed samples

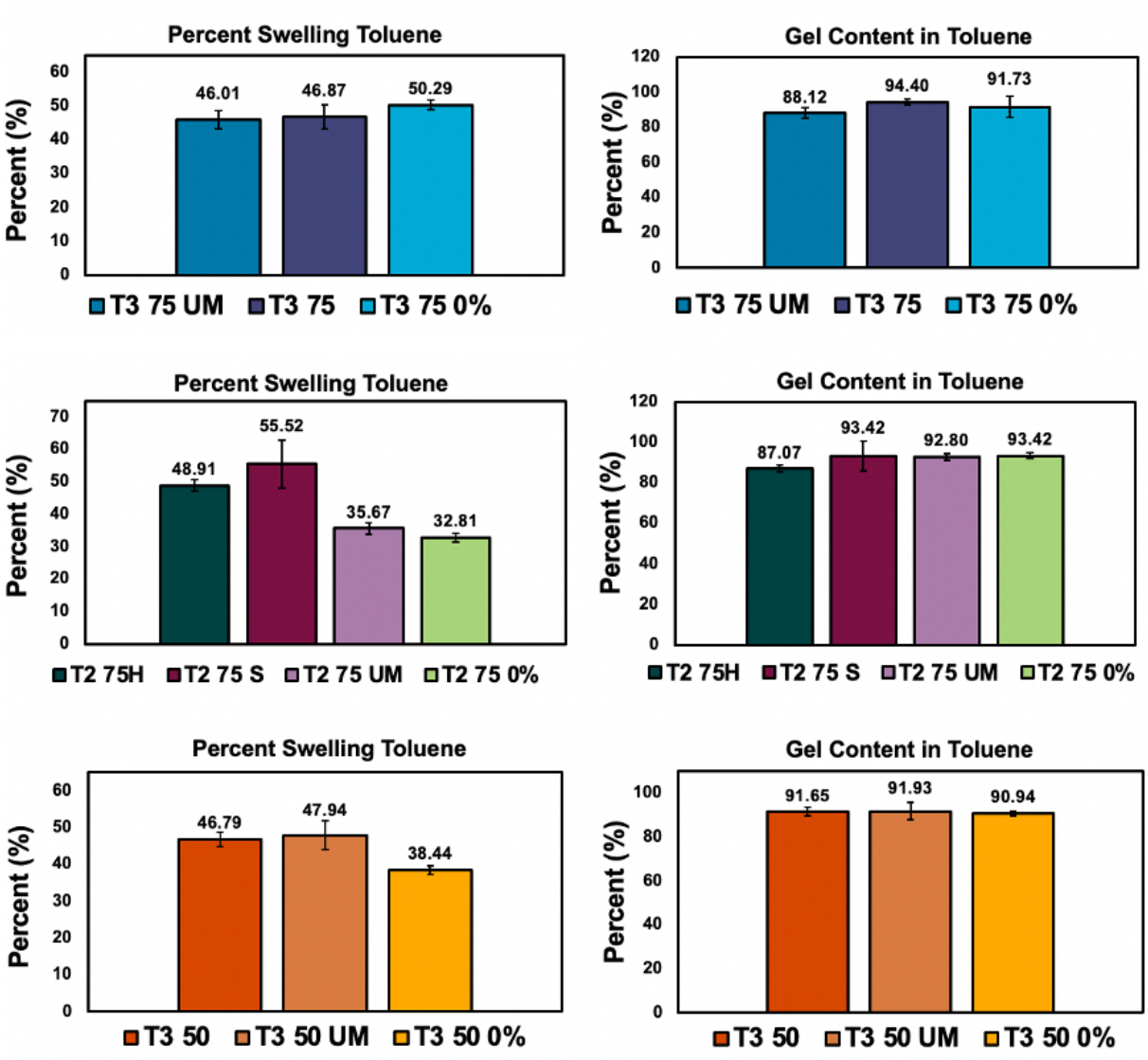

Figure S13. Swelling and gel content tests in toluene.

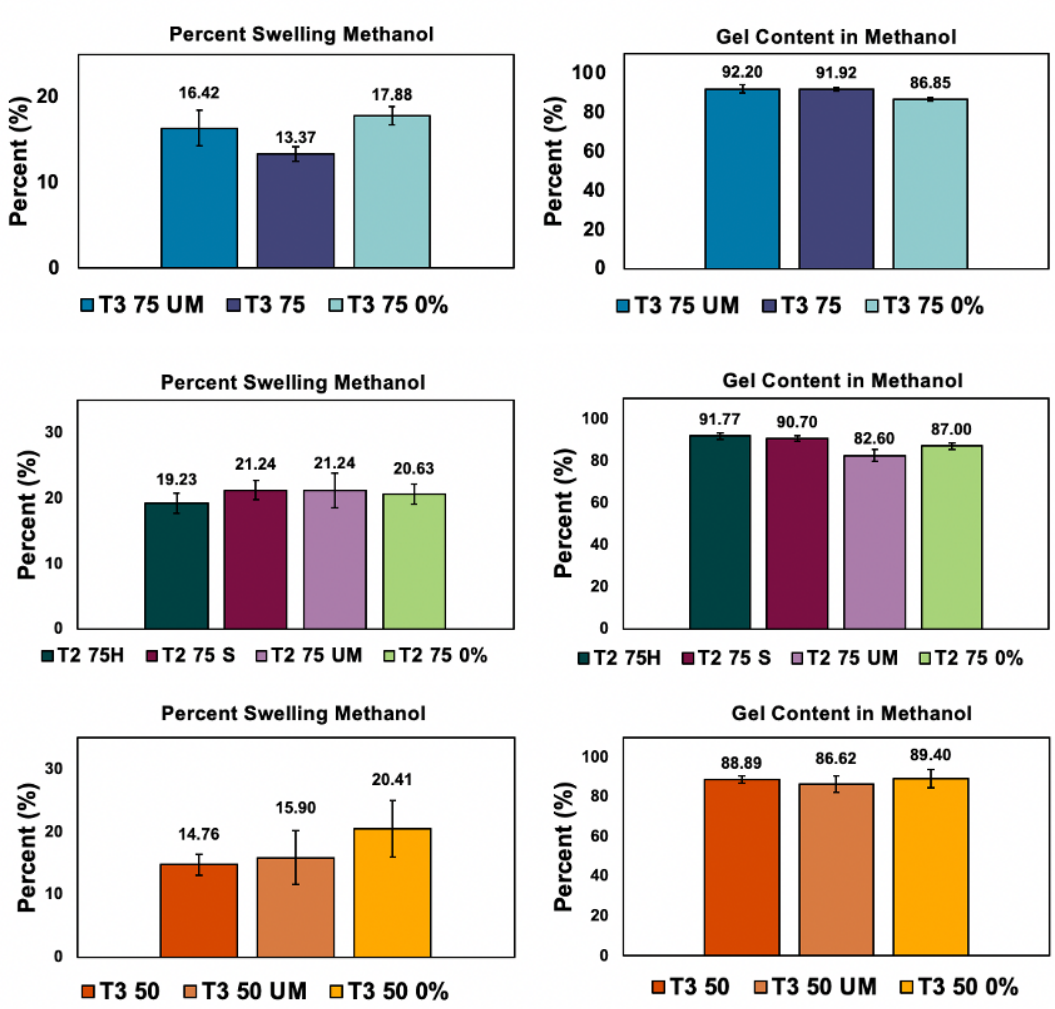

Figure S14. Percent swelling and gel content tests in methanol. The formulations show little swelling in methanol, but the formulations with LMA swell the least.

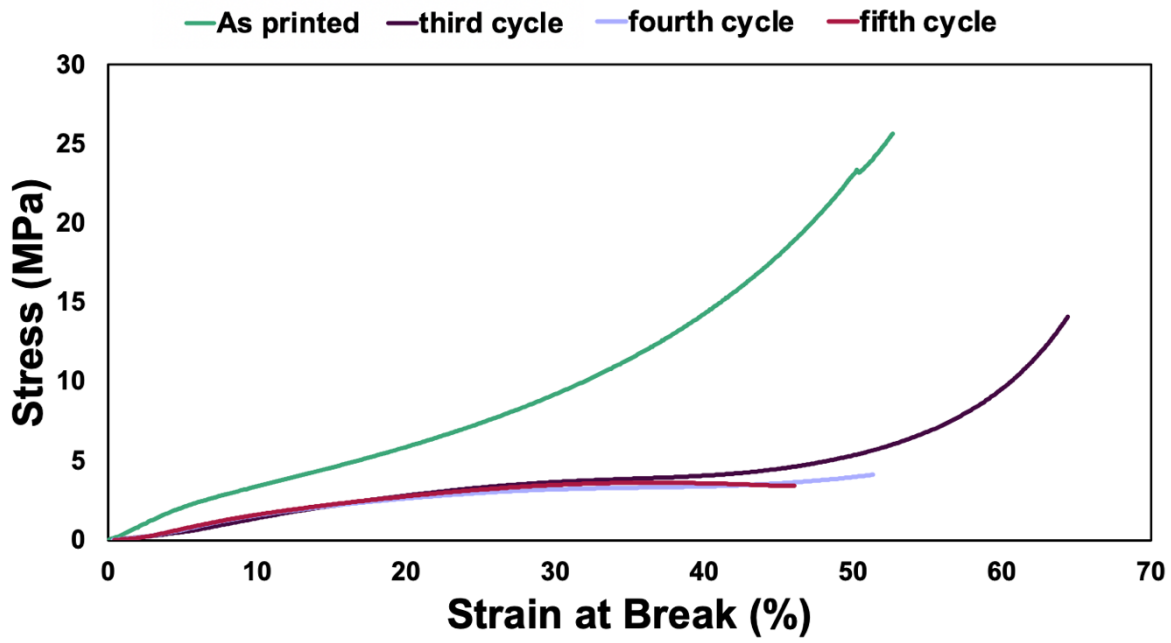

Figure S15. Stress-strain plots for the compression tests of the as printed, and reprocessed T2 75 Hard samples after multiple successive rounds of mechanical grinding and pressing with a Carver hydraulic press. Initially, there is a loss in the mechanical properties, but the successive reprocessing does little to change the properties except for the strain at break.

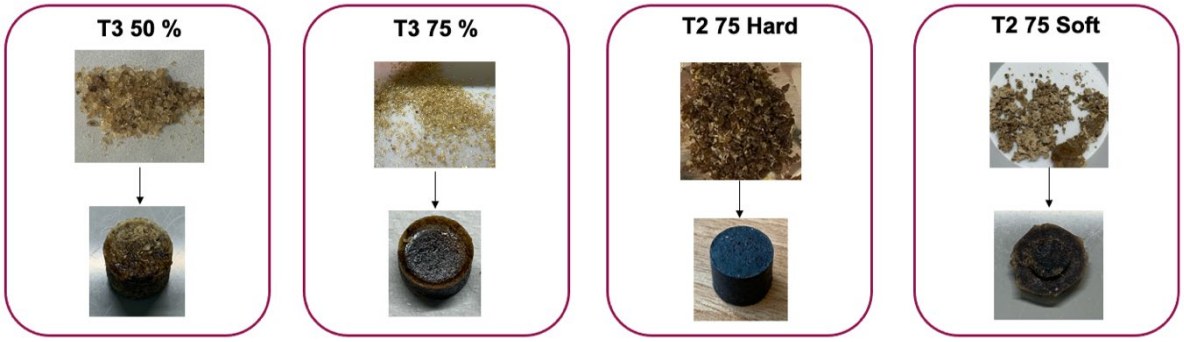

Figure S16. Images of each printed sample after being mechanically ground and reprocessed into discs for compression testing. All of the formulations, with the exception of T3 50, could be remolded into cylinders with uniform structures and even reincorporation of the polymer particles. All samples were pressed at 2,000 psi (2 metric tons) at 140°C for 4h.

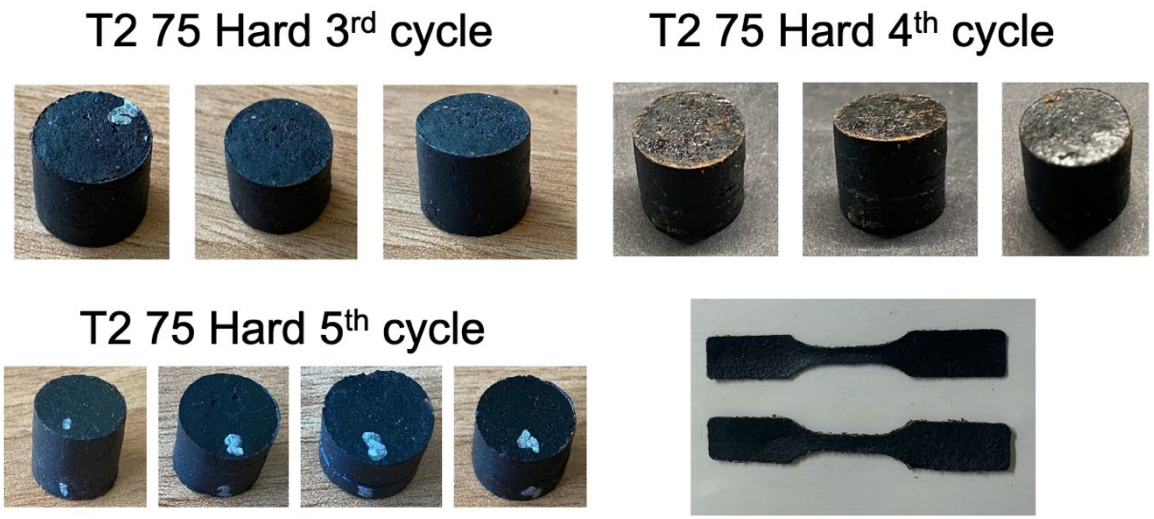

Figure S17. Samples of T2 75 hard after the 3rd, 4th and 5th cycles of reprocessing, and dog bones showing the ability to make fully incorporated materials. The formulations were mechanically ground and molded using a Carver hydraulic press and were compressed at 2,000 psi (2 metric tons) at 140°C for 4h.